Korean J. Chem. Eng., 32(7), 1267-1272 (2015)
DOI: 10.1007/s11814-014-0325-7

pISSN: 0256-1115
eISSN: 1975-7220

Characterization of supported Ni catalysts for aqueous-phase reforming of glycerol

Hong-Joo Lee*, Gwan Su Shin, and Young-Chul Kim***,†**

*Department of Bioenergy Science and Technology, Chonnam National University, Gwangju 500-757, Korea
**Department of Advanced Chemical Engineering, Chonnam National University, Gwangju 500-757, Korea
***Faculty of Applied Chemical Engineering and the Research Institute for Catalysis,
Chonnam National University, Gwangju 500-757, Korea
(*Received 13 June 2014 • accepted 4 November 2014*)

Abstract−The aqueous phase reforming (APR) over supported nickel-based catalysts was investigated as a feasibility study for hydrogen production from glycerol, byproduct of biodiesel produced by trans-esterification of triglycerides. Four different Ni-supported catalysts ($Ni/LaAlO_3$, Ni/CeO_2, Ni/MgO, and Ni/MgAl) were examined for the glycerol reforming in terms of the catalytic activities and the level of resistance. The APR of glycerol over Ni-supported catalysts showed that the conversion of glycerol to gas and H_2 selectivity were strongly dependent on the support and amount of Ni loading. A perovskite type catalyst, $Ni/LaAlO_3$, showed the highest reforming performance and good stability. A perovskite-type catalyst showed the glycerol conversion to 36% and the maximum value of H_2 and CO_2 selectivity to 96% and 81%. And the reforming gas composition in gas phase was measured to H_2 61%, CO_2 32%, CH_4 6%, and CO 1% in the APR over $Ni/LaAlO_3$. Comparison results of the reported results showed that Ni supported catalysts in the present study showed good performance for the APR to produce hydrogen from renewable resources.

Keywords: Aqueous Phase Reforming, Nickel-based Catalysts, Glycerol, Hydrogen, Reforming

INTRODUCTION

The importance of the use of hydrogen has considerably increased over the last decade as one of the renewable energy source carriers [1]. Hydrogen is a potential non-carbon based energy system considered as a clean and efficient energy carrier to replace fossil fuels since its combustion produces only water as byproduct [2,3].

Several biomass-derived oxygenated compounds, such as alcohols (methanol, ethanol) and polyols (ethylene glycol, glycerol, and sorbitol), have been considered as hydrogen reforming feedstocks. Glycerol ($C_3H_5(OH)_3$) (1,2,3-propanetriol), a byproduct of biodiesel produced by trans-esterification of triglycerides, has drawn much attention because the production of large amounts of glycerol is one of the bottlenecks to decrease the biodiesel production process [4-6].

The production of hydrogen using a proper reforming process is considered a promising way to utilize glycerol produced from biodiesel production process [7]. Many reforming techniques have been studied for the production of hydrogen from glycerol: steam reforming (SR), partial oxidation (POX), autothermal reforming (ATR), aqueous phase reforming (APR), and the supercritical water reforming process [8-10]. Among reforming processes, the APR process has attracted interest because it can operate at relatively higher pressures and lower temperature compared to SR [10]. The energy required to vaporize water can be saved because the reforming process takes place in an aqueous phase. Furthermore, APR reforming employs the water gas shift reaction, resulting in the CO production to a sufficiently low level in the reforming gas [11]. Furthermore, the formation of hydrogen proceeds by successive dehydration/reduction steps, leading to complete reduction of glycerol. The stoichiometry of the reaction pathways during the glycerol reforming process is as follows:

$$\text{Reforming:} \quad C_3H_5(OH)_3 \rightarrow 3CO + 4H_2 \tag{1}$$

$$\text{Water gas shift:} \quad 3CO + 3H_2O \rightarrow 3CO_2 + 3H_2 \tag{2}$$

$$\text{Overall:} \quad C_3H_5(OH)_3 + 3H_2O \rightarrow 3CO_2 + 7H_2 \tag{3}$$

In general, the selection of a proper catalyst is important in reforming processes [12]. Various catalysts have been investigated to minimize deactivation during the APR process of hydrogen from glycerol. Noble metal catalysts, such as Ni, Pt, and Pd, are commonly used for the APR of hydrogen because they are more active and less susceptible to carbon deposition than non-noble metal catalysts. In addition, they show high hydrogen production efficiency due to water gas shift reaction [13].

Among the catalysts, nickel-based catalysts provide high mechanical strength and chemical stability. However, severe deactivation under the reaction conditions in the APR of glycerol is one of the major problems associated with nickel-supported catalysts [14]. Therefore, it is important to choose catalysts with low level of coking and high activity. In the present study, the catalytic activity and the level of resistance to the coking of Ni-supported catalysts ($Ni/LaAlO_3$, Ni/CeO_2, Ni/MgO, and Ni/MgAl) were investigated as a feasible study for hydrogen production from renewable resources. In addition, the influence of Ni loading on catalytic performance was investigated using four catalysts. Catalyst properties, such as structure, surface area, pore size, condition of metal surface, mor-

†To whom correspondence should be addressed.
E-mail: youngck@chonnam.ac.kr

phology, and their stability, were characterized under the revealing conditions.

EXPERIMENTAL METHODS

1. Preparation of Ni-supported Catalysts

Four different types of Ni-supported catalysts, Ni/$LaAlO_3$, Ni/CeO_2, Ni/MgO, and Ni/MgAl, were prepared and the feasibility of glycerol forming was examined in terms of the catalytic activities of APR and the level of resistance. A perovskite type Ni/$LaAlO_3$ catalyst was prepared using the deposition-precipitation of Na_2CO_3 and NH_4OH [15]. It was dried at 100 °C in an oven for 12 h, followed by calcination at 400 °C for 2 h then dried again at 850 °C for 11 h under air atmosphere. Three other Ni-supported catalysts, Ni/CeO_2, Ni/MgO, and Ni/MgAl, were prepared by precipitation using aqueous nickel nitrate hexahydrate, $Ni(NO_3)_2 \cdot 6H_2O$ (Sigma-Aldrich, St. Louis, MO), which were found elsewhere [15]. They were dried at 100 °C for 12 h in an oven, followed by calcination at 400 °C for 5 h under air atmosphere.

2. Characterization of Ni-supported Catalysts

The composition of the Ni loading on the calcined catalysts was determined by using inductively coupled plasma atomic emission spectroscopy (ICP-AES) (Perkin-Elmer Optima 3300 DV). The reduction of examined catalysts was monitored by a chemical analyzer, BEL-CAT (BEL, Japan), and temperature-programmed reduction (TPR) from an ambient temperature to 900 °C at a rate of 5 °C/min in the environment of 5% H_2 flow (balance N_2). The weight loss of each catalyst and the amount of adsorbed compounds were determined by thermogravimetry (TG) with a Mettler Toledo, SKA 851^e. Thermogravimetric analysis was carried out by increasing temperature from ambient temperature to 1,000 °C at a rate of 5 °C/min in N_2 flow.

The X-ray diffraction (XRD) patterns of the catalysts were recorded by using a Rigaku powder diffraction unit (DMAX 100) using monochromatized Cu Kα radiation. The diffraction patterns were identified and the analyzed results were compared with the provided database. The specific surface area of the supports was determined by nitrogen adsorption at −196 °C with a NanoPorosity-XQ. The samples were pre-treated under N_2 atmosphere at 200 °C for 10 h before the surface area measurements. The chemical state of each catalyst was analyzed by X-ray photoelectron spectroscopy (XPS) by using a Multilab 200 equipped with an electro analyzer and an Al Kα X-ray source.

The morphology of the surface, structure, distribution, and agglomeration of catalysts were observed with electron microscopes. The morphology of the samples was examined by field emission scanning electron microscopy (FE-SEM) (S-4700, Hitachi, Japan) and the metal particle distribution of the catalysts was determined by transmission electron microscopy (TEM) (JEN-2000FXII, JEOL, Japan) at an accelerating voltage of 200 kV.

3. Catalytic Reactions of Ni-supported Catalysts

For the catalytic activity measurements, about 1.0 g of catalyst was placed in a quartz glass tube of 16 mm inner diameter and 400 mm length. The reactant, the mixture of H_2O and glycerol with the ratio of 85/15 (wt%), was supplied through a preheater. The temperature of the reactor was measured by the Cr-Al thermocouple in the center of the reactor. Before the catalytic reaction, the reactor was conditioned with the H_2 flow at 550 °C for 2 h.

The APR of 15 wt% glycerol solution was conducted in a continuous flow fixed-bed stainless steel reactor for 20 h at the fixed liquid hourly space velocity (LHSV) of 5 h^{-1}. A back pressure regulator was used for all experiments to maintain constant pressure in the reactor.

Gas species and their composition in the gas phase were analyzed by on-line gas chromatography (Shimadzu 14B) using Hayesep C packed column (1/8″ x 3 m, 80-100 mesh) and Hayesep D packed column (1/8″ x 3 m, 100-120 mesh) with a thermal conductivity detector (TCD). Liquid phase effluent from the reactor was collected during the reaction, and the species and composition were analyzed by gas chromatograph-mass spectrometry (HP 6890/5973 GC-MS). The conversion of glycerol to gas and the selectivity of gas species were estimated using the following equations:

Glycerol conversion to gas (%)

$$= \frac{\text{mole amount of C components in reformate}}{\text{total mole amount of C in glycerol}} \times 100 \quad (4)$$

Selectivity of the component i (%)

$$= \frac{\text{C moles produced species i}}{\text{C moles produced in gas phase}} \times 100 \quad (5)$$

H_2 selectivity (%)

$$= \frac{\text{H}_2 \text{ moles produced}}{\text{C moles produced in gas phase}} \times (3/7) \times 100 \quad (6)$$

RESULTS AND DISCUSSION

1. Characterization of the Prepared Catalysts

The pore properties of the prepared catalysts were characterized by nitrogen adsorption-desorption isotherms (Table 1). The mean sizes of the particles in the calcined catalysts were measured to 1.3-1.4 nm, irrespective of the different types of catalysts. And the estimated values of the surface area and total pore volume varied from 10 to 26 m^2/g and from 0.01-0.09 cm^3/g, which are somewhat low values compared with previous results [15]. It is thought that the difference of those values was small to explain the catalysts' properties, even though the catalysts showed somewhat different values.

Fig. 1 represents the XRD patterns of four different catalysts with 15 wt% Ni loading. As seen, diffraction peaks of NiO are not clearly observed in the Ni/$LaAlO_3$ and Ni/CeO_2 catalysts due to the well dispersed Ni catalysts. Characteristic peaks for MgO, periclase, and $MgNiO_2$ were observed, as shown in the figure.

The XRD patterns of the perovskite type Ni/$LaAlO_3$ catalyst were measured with different Ni loadings. Characteristic peaks of NiO

Table 1. Physical-chemical properties of the prepared catalysts

Catalyst	BET surface area (m^2/g)	Total pore volume (cm^3/g)	Mean pore size (nm)	Ni (wt%)
15 wt% Ni/$LaAlO_3$	10	0.01	1.3	14.93
15 wt% Ni/MgAl	26	0.07	1.3	14.87
15 wt% Ni/CeO_2	18	0.01	1.4	14.24
15 wt% Ni/MgO	20	0.09	1.3	14.59

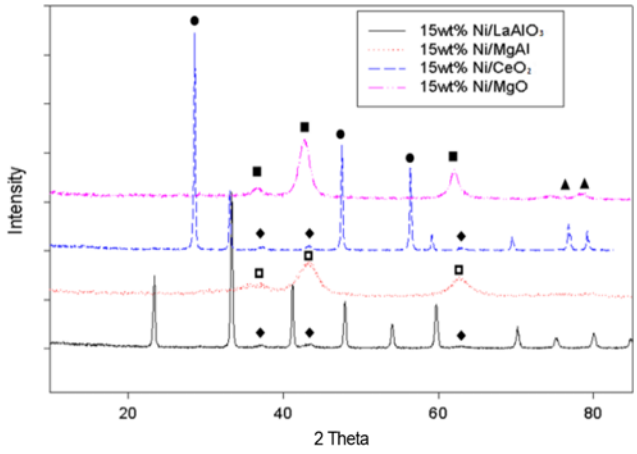

Fig. 1. X-ray diffraction patterns of various catalysts (◆: NiO, ●: CeO_2, ■: MgO, □: Periclase, ▲: $MgNiO_2$).

were clearly observed in the 20 wt% $Ni/LaAlO_3$, which appeared at 37°, 43°, and 63° (see Fig. 1 in Supplementary Data). Characteristic reflections of $Ni/LaAlO_3$ catalysts with loadings lower than 20 wt% were not clearly detected, suggesting that these species were well dispersed in the low Ni loading catalysts.

2. Catalytic Performance of Hydrogen Production

Composition changes of the catalysts were investigated and Fig. 2 shows the time course of the composition of the gas phase in the Ni-supported $LaAlO_3$ catalyst. After 3 h operation, the selectivity of gas species showed stable values for the $Ni/LaAlO_3$ catalyst. The high selectivity of hydrogen and CO_2 was observed to be significantly high, while the CO selectivity was very low under the tested conditions.

The influence of the support on the catalytic performance was investigated for four different catalysts with 15% Ni-loaded supports ($Ni/LaAlO_3$, Ni/MgAl, Ni/CeO_2, and Ni/MgO). Table 2 shows the glycerol conversion to gas and the selectivity of gas species over $Ni/LaAlO_3$ catalysts with different Ni loadings. The $Ni/LaAlO_3$ with Ni loading of 15 wt% showed higher glycerol conversion to gas and H_2 selectivity. In addition, the lowest CO selectivity was observed in the APR over the 15 wt% $Ni/LaAlO_3$ catalyst, which is related to water gas shift reaction (2): $Ni/LaAlO_3$ catalyst with 15 wt% showed high conversion (35.8%), high selectivity of CO_2 (80.8%) and low selectivity of CO (2.7%). In this study, 20 wt% $Ni/LaAlO_3$ catalyst showed lower conversion and lower selectivity of CO_2, thus resulting in high selectivity of CO. The 20 wt% $Ni/LaAlO_3$ catalyst showed lower glycerol conversion and hydrogen selectivity than 15 wt% $Ni/LaAlO_3$, which may be related to poor dispersion at Ni loading of 20 wt%, which was explained before.

Glycerol conversion to gas and the selectivity of gas species of the different catalysts are shown in Table 3. Among catalysts, $Ni/LaAlO_3$ showed much higher glycerol conversion to gas (36%) and hydrogen selectivity (67%) than Ni-supported catalysts supported on CeO_2, MgAl and MgO. The highest reforming performance of the $Ni/LaAlO_3$ catalyst may be related to its chemical stability, which can be observed in weight change with increasing temperature [16, 17]. The composition of gas species (H_2, CO, CH_4, and CO_2) was 61%, 1%, 6%, and 32%, respectively, in the APR of glycerol over $Ni/LaAlO_3$. Meanwhile, the Ni-supported CeO_2 shows the lowest conversion of glycerol to gas, half that of $Ni/LaAlO_3$, which accords with previous results [12,18]. Among examined catalysts, the Ni/CeO_2 showed the highest selectivity of CO (37%) with the high

Table 2. Glycerol conversion and gas product selectivity for the $Ni/LaAlO_3$ with different loading

		5 wt% $Ni/LaAlO_3$	10 wt% $Ni/LaAlO_3$	15 wt% $Ni/LaAlO_3$	20 wt% Ni /$LaAlO_3$
Conversion of glycerol to gas (%)		28.9	33.9	35.8	30.1
Selectivity (%)	H_2	55.0	54.3	67.2	48.2
	CO	34.1	14.31	2.7	59.1
	CH_4	25.5	18.1	16.5	14.7
	CO_2	40.5	67.65	80.8	26.3

Experimental condition: 15 wt% glycerol, 250 °C, 20 bar, and LHSV 5 h^{-1}

Table 3. Catalytic performances of glycerol reforming over Ni-based catalysts with different support type

		15 wt% $Ni/LaAlO_3$	15 wt% Ni/MgAl	15 wt% Ni/CeO_2	15 wt% Ni/MgO
Conversion of glycerol to gas (%)		35.8	32.5	17.3	32.1
Selectivity (%)	H_2	67.2	36.2	95.7	60.3
	CO	2.7	0.9	36.8	1.0
	CH_4	16.5	39.9	7.1	24.2
	CO_2	80.8	59.2	56.1	74.8
Composition (%)	H_2	61.0	46.7	68.5	56.8
	CO	1.1	0.7	11.5	0.7
	CH_4	6.3	18.4	2.2	10.9
	CO_2	31.6	34.2	17.8	31.6

Experimental condition: 15 wt% glycerol, 250 °C, 20 bar, and LHSV 5 h^{-1}

Table 4. Comparison of various APR of glycerol for hydrogen production

Catalyst	Operating parameters	Product in gas phase	Ref
Pt/Al_2O_3	Temperature: 225 and 265 °C Pressure: 29 and 56 bar Glycerol concentration: 1 wt%	Glycerol conversion: 83% (225 °C), 99% (265 °C)	[1]
Pt supported on Al_2O_3	Temperature: 250 °C Pressure: 20 bar Glycerol concentration: 10 wt%	Glycerol conversion: 38-45% Hydrogen selectivity: 85-87%	[31]
Pt/Al_2O_3	Temperature: 180-220 °C Pressure: 11.4-25.0 bar Glycerol concentration: 5-10 wt%	Glycerin conversion: 65% (glycerol 5 wt%) Hydrogen selectivity: about 90% (glycerol 5 wt%)	[6]
Ni/Al_2O_3 modified with Mg, Ce, La, Zr	Temperature: 225 °C Pressure: 30 bar Glycerol concentration: 1 wt%	Glycerol conversion: 15-37% Composition in gas phase: H_2 32-48%, CO_2 31-42%, CH_4 12-37%	[24]
Ni, Pt, and $PtNi/Al_2O_3$ and La-Al_2O_3	Temperature: 225-240 °C Pressure: 40 bar Glycerol concentration: 10 wt%	Glycerol conversion: 13-27% (225 °C), 14-52% (240 °C)	[14]
Pt/Al_2O_3, ZrO_2, MgO, CeO_2	Temperature: 225 °C, Glycerol concentration: 1 wt% Pressure: 23 bar	Glycerol conversion: 13-26% Composition in gas phase: H_2 63-72%, CO_2 26-33%, CO below 0.05%	[12]
Pt loaded MgO, Al_2O_3, CeO_2, TiO_2, SiO_2	Temperature: 225 °C, Glycerol concentration: 5 wt% Pressure: 27.6 bar	Glycerol conversion: 20-48% Composition in gas phase: H_2 58-62%, CO_2 34-38%, CO 0.1-1.2% H_2 selectivity: 60-70%	[32]
3%Pt-Re/C (1 and 3% Re)	Temperature: 225 °C, Glycerol concentration: 10 wt% Pressure: 28 bar	Glycerol conversion: 5-89% H_2 selectivity: 14-56%	[33]
Ni-Cu from hydrotalcite	Temperature: 250, 270 °C, Glycerol concentration: 10 wt% Pressure: 38-52 bar	Glycerol conversion: max 60% (270 °C) H_2 selectivity: 80% (250 °C)	[13]
Ni supported $LaAlO_3$, CeO_2, MgO, and MgAl	Temperature: 250 °C Glycerol concentration: 15 wt% Pressure: 20 bar	Glycerol conversion: max 36% Selectivity: H_2 max 96%, CO_2 max 81% Composition in gas phase: H_2 61%, CO_2 32%, CH_4 6%, CO 1% for $Ni/LaAlO_3$	In this study

concentration of 11%, which undergoes water gas shift reaction at the examined temperature (250 °C) [19-21].

Table 4 summarizes reported results on the glycerol reforming by APR using various types of catalysts. As seen in the table, glycerol conversion to gas shows the strong dependence on the type of catalysts and the experimental conditions. In this study, a relatively high amount of glycerol was supplied as a feedstock for the hydrogen reforming, and the glycerol conversion reached 36%, somewhat high compared to the results shown in the table. The maximum values of H_2 and CO_2 selectivity for the Ni-supported catalysts were measured to be 96% and 81%, respectively. Comparison results in the table showed that Ni-supported catalysts showed good APR performance to produce hydrogen production from glycerol.

3. Characterization of the Reacted Catalyst Properties

In general, the activity of a catalyst is related to the amount of carbon deposition as well as the dispersion and particle size since carbon deposition gives significant effects on the stable operation and high conversion of hydrocarbons [22]. In this study, the surface change was analyzed from SEM and TEM images of fresh and reacted catalysts of Ni/MgO, $LaAlO_3$, CeO_2, and MgO catalysts, respectively. SEM analyses of the fresh catalysts showed a plane-like structure with a high surface area (see Fig. 2 in Supplementary Data). After the catalytic reaction, the structure of the metal oxides changed due to sintering during the reforming reaction [15].

TEM images of the Ni phase showed particles localized especially in the pores of the support (see Fig. 3 in Supplementary Data). The Ni particle size was measured as 10-15 nm in the TEM images. Significant changes in carbon morphology and structure were also observed after the APR experiments. In addition, some agglomerated carbon particles formed on the Ni-supported catalysts after the APR of glycerol using Ni/MgAl, Ni/CeO_2, and Ni/MgO under the tested reaction conditions. Through the TEM analysis of the $Ni/LaAlO_3$ catalyst, it was observed that the amount of carbon deposit was as small as a form of a fiber type after the reforming process.

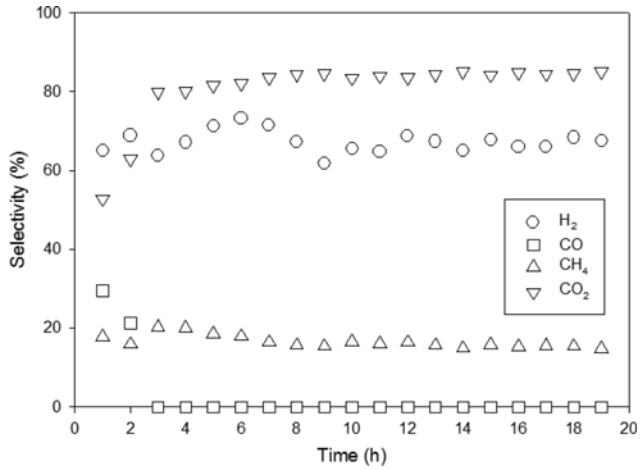

Fig. 2. Time course of gas species selectivity for $Ni/LaAlO_3$ catalyst (reaction conditions: 250 °C, 20 bar, and 5 h^{-1}).

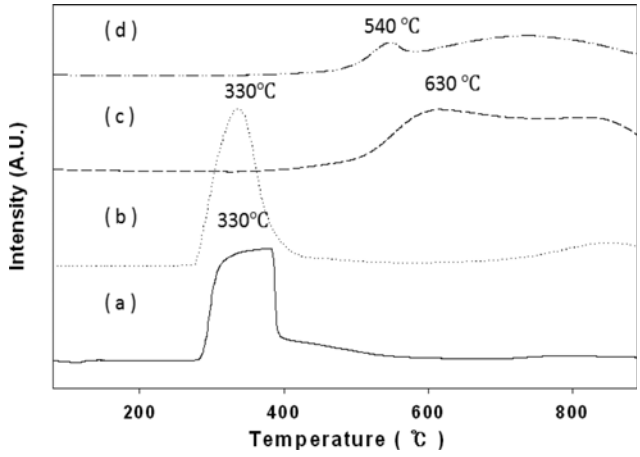

Fig. 3. TPR analysis of Ni-based catalysts with different supports: (a) $Ni/LaAlO_3$ (b) Ni/CeO_2 (c) Ni/MgAl, and (d) Ni/MgO.

The previous studies showed that carbon deposits in the form of the fiber type deposition had little effect on the catalyst activity due to the low amount of fiber type deposited carbon on the surface, while the deposit form of graphite significantly affect the catalyst activity [15,23].

The reduction of catalysts was examined by using TPR (Fig. 3). The most prominent peak was observed at around 330 °C due to the reduction of Ni^{2+} in the NiO phase for $Ni/LaAlO_3$ and Ni/CeO_2. The reduction peak appearing at a high temperature is related to the reduction of highly dispersed non-stoichiometric amorphous nickel aluminate spinels [24]. The reduction peak was observed at a lower temperature for the $Ni/LaAlO_3$ and Ni/CeO_2 catalysts in the TPR results.

Decomposition behaviors of the fresh and used catalysts were compared through thermogravimetric analysis [25]. The TGA profiles for the Ni supported catalysts are shown in Fig. 4. Weight decrease in the figure started at around 330 °C for the Ni-loaded MgO and MgAl catalysts, indicating these catalysts became deactivated during the APR process [26]. However, small changes in the thermogravimetric results of the $Ni/LaAlO_3$ and Ni/CeO_2 catalysts were

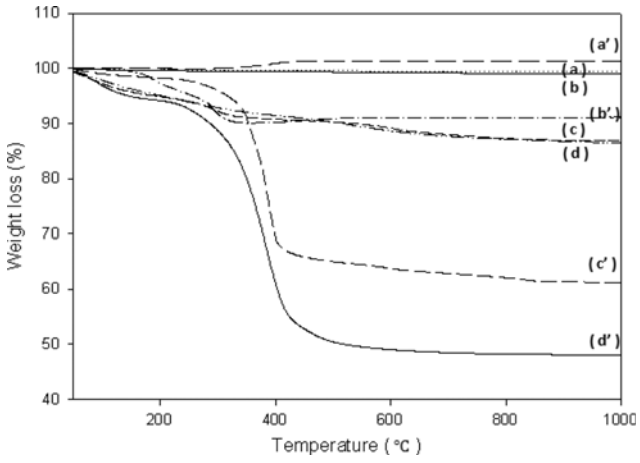

Fig. 4. TGA analysis of Ni/MgO, $LaAlO_3$, CeO_2 and MgAl catalysts: Fresh $Ni/LaAlO_3$ (a) and reacted $Ni/LaAlO_3$ (a′), fresh Ni/CeO_2 (b) and reacted Ni/CeO_2 (b′), fresh Ni/MgO (c) and reacted Ni/MgO (c′), fresh Ni/MgAl (d) and reacted Ni/MgAl (d′).

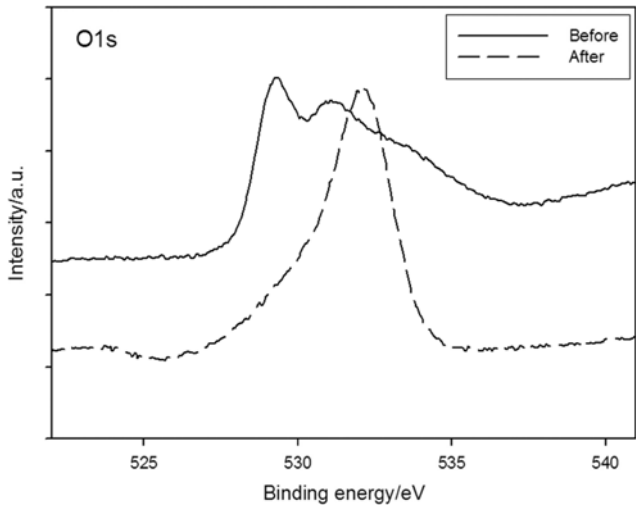

Fig. 5. Change in the chemical state after the reaction in XPS analysis of $Ni/LaAlO_3$ catalyst.

observed due to a lower amount of coke formation compared to the Ni/MgO and Ni/MgAl catalysts, which was observed in the TEM analysis. The amount of the lost weight increased after the APR reaction in the Ni/CeO_2 catalyst due to the easier recovery of lattice oxygen compared with that of CeO_2. The high resistance to coking in the $Ni/LaAlO_3$ catalyst might be partly due to the migration of mobile oxygen from the $LaAlO_3$ support to the metallic nickel particles through TGA and TPR [26-28].

Generally, XPS is used to determine the chemical state of materials and their surface proportions in fresh and used catalysts. Fig. 5 compares XPS data for the oxygen 1s region of binding energy for the fresh and used $Ni/LaAlO_3$ catalysts. These spectra show the two main peaks with binding energy values at ca. 529 eV and ca. 531 eV [25]. The lower binding energy peak can be assigned to the lattice oxygen species, O^{2-}, a similar result in previous studies [29, 30]. Meanwhile, the higher binding energy peak can be related to

an adsorbed oxygen species or molecular water adsorbed on the surface. As seen, the amount of lattice oxygen (at 529 eV) was greater than that of absorbed oxygen (at 531 eV) before the APR reaction. However, the lattice oxygen changed dramatically after the reforming reaction [12]. Through XPS results, lattice oxygen in the Ni/$LaAlO_3$ catalyst was maintained during the reforming reaction, which explains the stability of the active site in a catalyst structure.

CONCLUSIONS

Interest in the aqueous phase reforming (APR) for hydrogen production from glycerol, byproduct of biodiesel, has increased because the reforming occurs in an aqueous phase with mild conditions, producing a low level of CO. In this study, four different Ni-supported catalysts (Ni/$LaAlO_3$, Ni/CeO_2, Ni/MgO, and Ni/MgAl) were prepared and catalyst properties such as structure, surface area, pore size, condition of metal surface, morphology, and their stability were characterized under the revealing conditions.

The APR of glycerol over Ni-supported catalysts showed that the conversion of glycerol to gas and H_2 selectivity were strongly dependent on the support and amount of Ni loading. The catalyst showed the glycerol conversion to 36% and the maximum value of H_2 and CO_2 selectivity to 96% and 81%. Among Ni-supported catalysts, a perovskite-type catalyst, Ni/$LaAlO_3$, showed higher glycerol conversion to gas and H_2 selectivity. It was shown that the high resistance to coking in the Ni/$LaAlO_3$ catalyst is related to the migration of mobile oxygen from the $LaAlO_3$ support to the metallic nickel particles. Also, the high stability of the active site in Ni/$LaAlO_3$ catalyst could be explained by small change of lattice oxygen in the catalyst. In the comparison of results with previous results on the APR of glycerol, the present study showed good APR performance to produce hydrogen production from glycerol. It was clearly shown through the study that a perovskite-type catalyst could be considered as one of the feasible APR catalysts for the hydrogen production from renewable resources.

ACKNOWLEDGEMENTS

This work was supported by the Priority Research Centers Program through the National Research Foundation of Korea (NRF) funded by the Ministry of Educations, Science and Technology (2009-0094055), and supported partly by the Ministry of Knowledge Economy of Korea and the Korea Institute of Science and Technology (KIST).

REFERENCES

1. R. D. Cortright, R. R. Davda and J. A. Dumesic, *Nature*, **418**, 964 (2002).
2. S. Kim and M. Kang, *J. Ind. Eng. Chem.*, **18**, 969 (2012).
3. M. Slinn, K. Kendall, C. Mallon and J. Andrews, *Bioresour. Technol.*, **99**, 5851 (2008).
4. Z. Y. Huang, C. H. Xu, C. Q. Liu, H. W. Xiao, J. Chen, Y. X. Zhang and Y. C. Lei, *Korean J. Chem. Eng.*, **30**, 587 (2013).
5. K. K. Pant, R. Jain and S. Jain, *Korean J. Chem. Eng.*, **28**, 1859 (2011).
6. N. Luo, X. Fu, F. Cao, T. Xiao and P. P. Edwards, *Fuel*, **87**, 3483 (2008).
7. S. Adhikari, S. D. Fernando and A. Haryanto, *Energy Convers. Manage.*, **50**, 2600 (2009).
8. M. Seong, M. Shin, J. H. Cho, Y. C. Lee, Y. K. Park and J. K. Jeon, *Korean J. Chem. Eng.*, **31**, 412 (2014).
9. R. R. Davda, J. W. Shabaker, G. W. Huber, R. D. Cortright and J. A. Dumesic, *Appl. Catal. A*, **43**, 13 (2003).
10. R. R. Davda, J. W. Shabaker, G. W. Huber, R. D. Cortright and J. A. Dumesic, *Appl. Catal. B*, **56** 171 (2005).
11. A. O. Menezes, M. T. Rodrigues, A. Zimmaro, L. E. P. Borges and M. A. Fraga, *Renewable Energy*, **36**, 595 (2011).
12. P. V. Tuza, R. L. Manfro, N. F. P. Ribeiro and M. M. V. M. Souza, *Renewable Energy*, **50**, 408 (2013).
13. A. Iriondo, J. F. Cambra, V. L. Barrio, M. B. Guemez, P. L. Arias, M. C. Sanchez-Sanchez, R. M. Navarro and J. L. G. Fierro, *Appl. Catal. B*, **106**, 83 (2011).
14. N. A. Merino, B. P. Barbero, P. Grange and L. E. Cadús, *J. Catal.*, **231**, 232 (2005).
15. S. S. Lim, H. J. Lee, D. J. Moon, J. H. Kim, N. C. Park, J. S. Shin and Y. C. Kim, *Chem. Eng. J.*, **152**, 220 (2009).
16. S. Barison, M. Battagliarin, S. Daolio, M. Fabrizio, E. Miorin, P. L. Antonucci, S. Candamano, V. Modafferi, E. M. Bauer, C. Bellitto and G. Righini, *Solid State Ionics*, **177**, 3473 (2007).
17. B. Dou, V. Dupont, G. Rickett, N. Blakeman, P. T. Williams, H. Chen, Y. Ding and M. Ghadiri, *Bioresour. Technol.*, **100**, 3540 (2009).
18. J. W. Shabaker, G. W. Huber, R. R. Davda, R. D. Cortright and J. A. Dumesic, *Catal. Lett.*, **88**, 1 (2003).
19. R. L. Manfro, A. F. da Costa, N. F. P. Ribeiro and M. M. V. M. Souza, *Fuel Process. Technol.*, **92**, 330 (2011).
20. B. Zhang, X. Tang, Y. Li, Y. Xu and W. Shen, *Int. J. Hydrogen Energy*, **32**, 2367 (2007).
21. B. Roy, H. Sullivan and C. A. Leclerc, *J. Power Sources*, **196**, 10652 (2011).
22. H. J. Lee, Y. S. Lim, N. C. Park and Y. C. Kim, *Chem. Eng. J.*, **146**, 295 (2009).
23. S. Natesakhawat, R. B. Watson, X. Wang and U. S. Ozkan, *J. Catal.*, **234**, 496 (2005).
24. A. Iriondo, V. L. Barrio, J. F. Cambra, P. L. Arias, M. B. Güemez, R. M. Navarro, M. C. Sánchez-Sánchez and J. L. G. Fierro, *Top. Catal.*, **49**, 46 (2008).
25. R. M. Navarro, M. C. Alvarez-Galvan, J. A. Villoria, I. D. González-Jiménez, F. Rosa and J. L. G. Fierro, *Appl. Catal. B*, **73**, 247 (2007).
26. K. Urasaki, Y. Sekine, S. Kawabe, E. Kikuchi and M. Matsukata, *Appl. Catal. A*, **286**, 23 (2005).
27. S. Adhikari, S. D. Fernando and A. Haryanto, *Renewable Energy*, **33**, 1097 (2008).
28. F. Frusteri, S. Freni, V. Chiodo, S. Donato, G. Bonura and S. Cavallaro, *Int. J. Hydrogen Energy*, **31**, 2193 (2006).
29. K. Tabata, Y. Hirano and E. Suzuki, *Appl. Catal. A*, **170**, 245 (1998).
30. R. Pereñíguez, V. M. González-DelaCruz, P. Holgado and A. Caballero, *Appl. Catal. B*, **93**, 346 (2010).
31. K. Lehnert and P. Claus, *Catal. Commun.*, **9**, 2543 (2008).
32. Y. Guo, U. M. Azmat, X. Liu, Y. Wang and G. Lu, *Appl. Energy*, **92**, 218 (2012).
33. D. L. King, L. Zhang, G. Xia, A. M. Karim, D. J. Heldebrant, X. Wang, T. Peterson and Y. Wang, *Appl. Catal. B*, **99**, 206 (2010).

Supporting Information

Characterization of supported Ni catalysts for aqueous-phase reforming of glycerol

Hong-Joo Lee*, Gwan Su Shin, and Young-Chul Kim***,†**

*Department of Bioenergy Science and Technology, Chonnam National University, Gwangju 500-757, Korea
**Department of Advanced Chemical Engineering, Chonnam National University, Gwangju 500-757, Korea
***Faculty of Applied Chemical Engineering and the Research Institute for Catalysis,
Chonnam National University, Gwangju 500-757, Korea
(*Received 13 June 2014 • accepted 4 November 2014*)

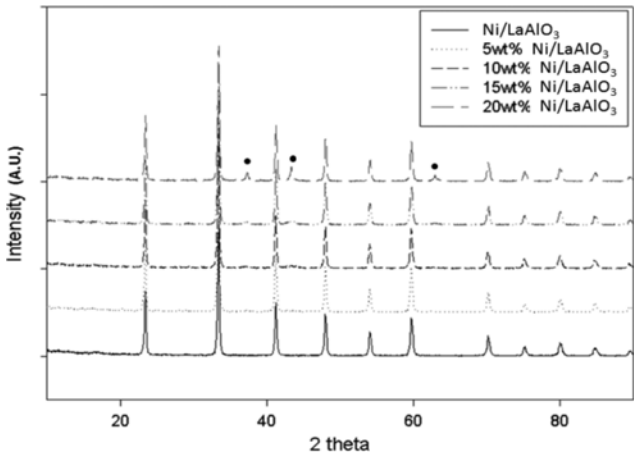

Suppl. Fig. 1. XRD patterns of $Ni/LaAlO_3$ catalysts with different Ni loadings and $LaAlO_3$ support (NiO).

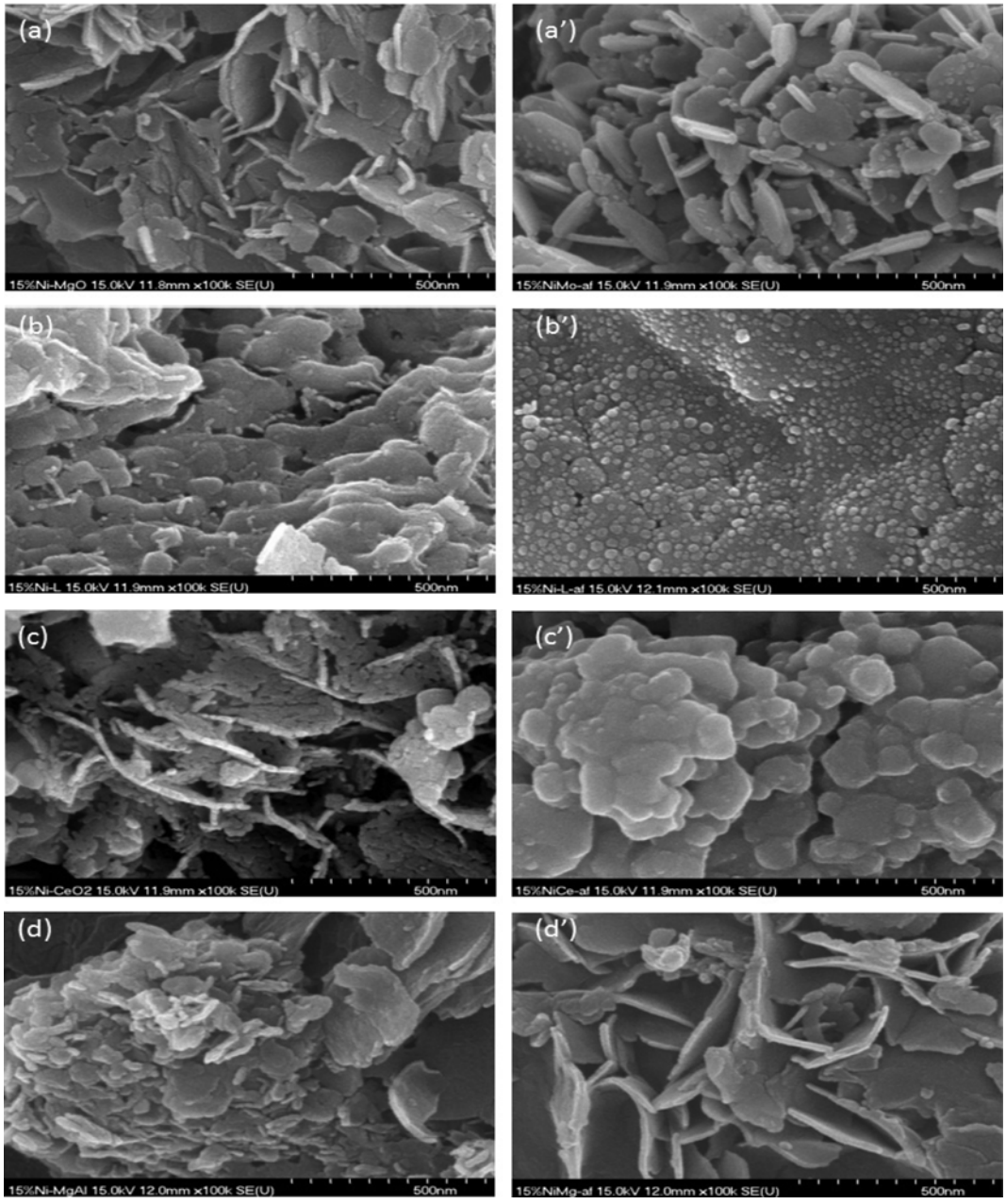

Suppl. Fig. 2. SEM images of Ni/MgO, $LaAlO_3$, CeO_2 and MgAl catalysts: Fresh Ni/MgO (a) and reacted Ni/MgO (a′), fresh Ni/$LaAlO_3$ (b) and reacted Ni/$LaAlO_3$ (b′), fresh Ni/CeO_2 (c) and reacted Ni/CeO_2 (c′) , fresh Ni/MgAl (d) and reacted Ni/MgAl (d′).

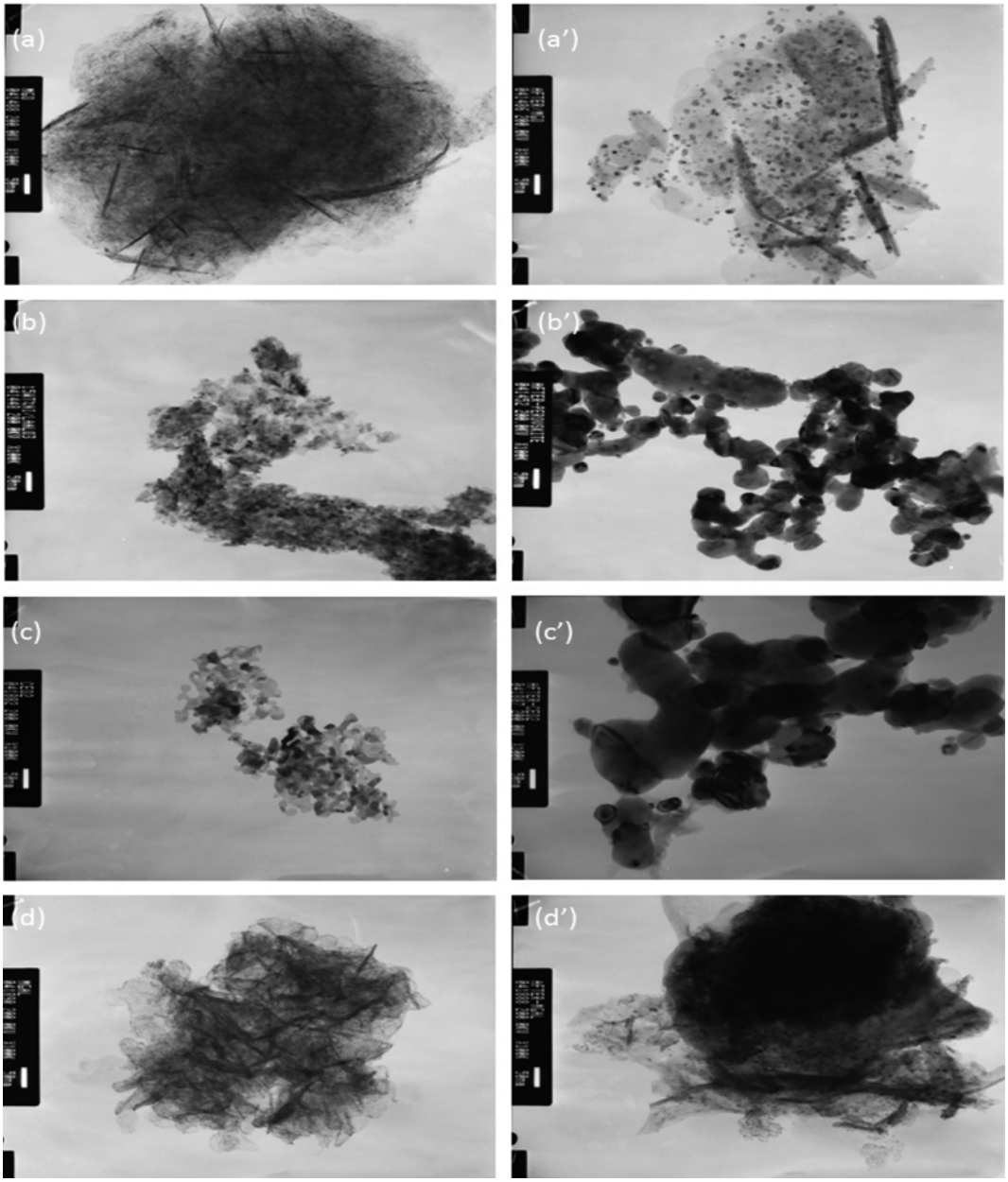

Suppl. Fig. 3. TEM images of Ni/MgO, $LaAlO_3$, CeO_2 and MgAl catalysts: Fresh Ni/MgO (a) and reacted Ni/MgO (a′), fresh Ni/$LaAlO_3$ (b) and reacted Ni/$LaAlO_3$ (b′), fresh Ni/CeO_2 (c) and reacted Ni/CeO_2 (c′) , fresh Ni/MgAl (d) and reacted Ni/MgAl (d′).